Journal of Molecular Structure 1292 (2023) 136078

Contents lists available at ScienceDirect

Journal of Molecular Structure

journal homepage: www.elsevier.com/locate/molstr

Pseudotetrahedral C_2-symmetrical Co/Zn(II)-achiral Schiff base complexes with Δ/Λ-chirality induction at-metal as a racemic mixture

Mohammed Enamullah [a,*], Imdadul Haque [a], Afsana Mim [a], Mohammad Khairul Islam [a], Baldeep K. Sidhu [b], David E. Herbert [b], Dennis Woschko [c], Christoph Janiak [c,*]

[a] Department of Chemistry, Jahangirnagar University, Dhaka 1342, Bangladesh
[b] Department of Chemistry, University of Manitoba, 144 Dysart Road, Winnipeg, Manitoba R3T 2N2, Canada
[c] Institut für Anorganische Chemie und Strukturchemie, Heinrich-Heine-Universität Düsseldorf, Universitätsstr. 1, Düsseldorf D-40225, Germany

ARTICLE INFO

Keywords:
Co/Zn(II)-Schiff base complexes
X-ray structures
Δ/Λ-chirality induction at-metal
Cyclic voltammetry and thermal analysis
DFT/TD-DFT calculations

ABSTRACT

Reaction of achiral Schiff base ligands 1-((X-phenylimino)methyl)naphthalen-2-ol {X = 2-ethyl (HL1) or 4-methyl (HL2)} with cobalt(II) or zinc(II) acetate provided the corresponding bis[1-((X-phenylimino)methyl) naphthalen-2-olato-k^2N,O]cobalt(II) or zinc(II) {X = 2-ethyl: M = Co (**1**) and Zn (**2**) or X = 4-methyl: M = Co (**3**) and Zn (**4**)} complexes. The molecules crystallize in the centrosymmetric space groups R–3 (**1**) and P–1 (**3** or **4**). Molecular structures determinations showed coordination of two molecules of the N,O-chelate ligands to the metal ion and formation of pseudotetrahedral complexes with C_2-symmetry. Furthermore, coordination of two unsymmetrical achiral N,O-chelates induces Λ/Δ-chirality at the metal atom as a racemic mixture in the centrosymmetric space groups. Structural analyses further reveal that incorporation of 2-ethyl (**1**) or 4-methyl (**3** or **4**) group on the N-bound phenyl ring leads to an increase of both the O1-M-O2 and N1-M-N2 bond angles on going from **1** to **3** or **4**, with the N1-M-N2 angle increasing to a much greater extent. The fair matching of the experimental and simulated powder X-ray diffraction patterns confirms the phase purity of bulk microcrystalline sample. Differential scanning calorimetry (DSC) results suggest an irreversible phase transformation from solid crystals to isotropic-liquids and subsequent thermal stability of the complexes. Cyclic voltammograms indicate a quasi-reversible two one electron charge transfer processes for **1** or **3** in N,N-dimethylformamide (DMF). Optimized geometry and excited state properties by density functional theory (DFT) and time dependent-density functional theory (TD-DFT) calculations correspond well to the experimental results.

1. Introduction

Transition metal(II)-Schiff bases complexes are of continued interest in view of syntheses, characterization, molecular structures, stereochemistry, photochromism, biological and catalytic activities [1–15]. Our recent studies on (a)chiral salicylaldiminate/naphthaldiminate Schiff bases ligands and their complexes with transition metal(II) ions revealed interesting nuances with respect to their coordination and molecular geometries, chiroptical properties, (dia)stereoselectivity, supramolecular architecture, molecular magnetism, thermal analyses and electrochemical properties [16–26]. Molecular structures determinations explored that coordination of the chiral/achiral N, O-chelate Schiff base ligands to the transition metal(II) ions provided nonplanar C_2-symmetrical [M(N,O)$_2$] complexes (N,O = deprotonated Schiff bases; M = Mn, Fe, Co, Ni, Cu and Zn) with pseudotetrahedral geometry. The nonplanar C_2-symmetrical complexes showed a special phenomenon of diastereoselection and Λ/Δ-chirality induction at-metal upon coordination to the metal ion by the chiral-Schiff base ligands, provided two diastereomers Δ-M(*R*-N,O)$_2$ and Λ-M(*R*-N,O)$_2$ {or Λ-M(*S*-N,O)$_2$ and Δ-M(*S*-N,O)$_2$} with one being thermodynamically favoured [16–26,27–33]. The phenomenon was also reported for some achiral-Schiff base ligands due to an asymmetric arrangement of the ligands around the metal ion in the complexes with nonplanar C_2-symmetry, gave a racemic mixture of two stereoisomers Δ-M(N,O)$_2$ and Λ-M(N,O)$_2$ [34,35]. The phenomenon is significantly influenced by the metal-ligand interactions and coordination sphere, ligand design and chirality, noncovalent inter-/intra-molecular interactions in the solid, solute-solvent interactions in solution, metal ion selection, ligand folding behaviours, variable time and temperature and crystallization protocol.

* Corresponding authors.
E-mail addresses: enamullah@juniv.edu (M. Enamullah), janiak@uni-duesseldorf.de (C. Janiak).

https://doi.org/10.1016/j.molstruc.2023.136078
Received 30 April 2023; Received in revised form 18 June 2023; Accepted 19 June 2023
Available online 24 June 2023

Few examples of the phenomenon reported in metal(II)-achiral Schiff base complexes include the reaction of N-2-(pyridyl)salicylaldimine with zinc(II) to give the chiral-at-metal Λ/Δ-Zn(II)-salicylaldiminates [34], which crystallized as a racemic conglomerate via spontaneous resolution. The X-ray molecular structures revealed that two salicylaldiminates form a pseudotetrahedral C_2-symmetrical complex with Λ/Δ-chirality induction at zinc atom. The complex assembles in *P* (right)- and *M* (left)-handed 4_1- and 4_3-helical chains in the chiral space groups $P4_12_12$ and $P4_32_12$, respectively via weak C−H···O hydrogen bonding interactions between the neighbouring molecules along the chain axis. Similar reaction with N-2-(4-methyl-pyridyl)-2-hydroxy-1-naphthaldimine gave the Λ/Δ-Zn(II)-naphthaldiminates complexes, where π–π interactions lead to an inversion-symmetric complex pair with opposite Λ- and Δ-configurations at the metal center [35].

We recently reported the syntheses, mesomorphic properties and molecular structures of square-planar Rh(I) [36] and Ni/Cu(II) [37] complexes with achiral Schiff base ligands ((X-phenylimino)methyl)--phenol/-naphthalen-2-ol [38–40]. Reaction of the same ligands with Co/Zn(II) provided the present bis[1-((X-phenylimino)methyl)naphthalen-2-olato-k^2N,O]cobalt(II) and zinc(II) {X = 2-ethyl: M = Co (**1**) and Zn (**2**); *X* = 4-methyl: M = Co (**3**) and Zn (**4**)} complexes. The molecular structures determinations for **1, 3** and **4** explored the formation of a pseudotetrahedral C_2-symmetrical complexes with Λ/Δ-chirality induction at-metal as a racemic mixture. It was further attempted to study the substituents effects of ligands on the molecular geometry, redox potential, thermal and PXRD analyses of the complexes. Geometry optimizations and excited state properties by DFT/TD-DFT were employed, which supported the experimental results of X-ray structures at solid and absorption spectra in solution.

2. Experimental

2.1. Chemicals and measurements

UV-vis. absorption spectra were obtained with a Shimadzu UV 1800 spectrophotometer in chloroform at 25 °C. IR spectra were recorded on a Nicolet iS10 (Thermo Scientific) spectrometer at ambient temperature. ^{1}H NMR spectra were run on a Bruker Avance DPX 400 spectrometer for compounds **2** in $CDCl_3$, **4** in DMSO-d_6 and *in-situ* reaction mixture of **1** with NaCN in DMSO-d_6 at 20 °C. Differential scanning calorimetry (DSC) was performed on a Shimadzu DSC-60 at 30-270 °C (ca. 5 °C above the m.p. to avoid any decomposition) with a heating rate of 10 K min^{-1}. Solid-state magnetic measurement ($\mu_{eff.}$) was carried out with the magnetic susceptibility balance MSB Mk1 (Sherwood Scientific Ltd.) at 25 °C. The molar conductance (Λ_m) was measured with a Mettler Toledo Fivego (Model F3) Conductivity metre in N,N-dimethylformamide (DMF) at 25 °C. An Epsilon™ Instruments (BASi) electrochemical analyzer was used for cyclic voltammetry experiments in DMF containing the tetra-N-butyl-ammonium-hexafluorophosphate (TBAP) as supporting electrolyte. A three-electrode measurement was performed at 25 °C with a platinum disk working electrode, platinum wire auxiliary electrode and Ag/AgCl reference electrode. The solution containing the sample and TBAP was deoxygenated for 10 min with nitrogen gas prior to use. Electron impact (EI) mass spectra were recorded with a Thermo-Finnigan TSQ 700 mass spectrometer. The spectra clearly show the isotopic distributions patterns for the complexes.

2.2. Syntheses of the complexes (1-4)

Two equivalents of HL1 (550 mg, 2 mmol) or HL2 (522 mg, 2 mmol) and $NaHCO_3$ (168 mg, 2 mmol) were dissolved in 10 mL of methanol. This solution was stirred for 10 min at room temperature. One equivalent of Co(II) or Zn(II) acetate (249 or 220 mg, 1 mmol) was then dissolved in 5 mL methanol and added into this mixture solution, which was continued to stir under room temperature. The color of the mixture solution changed rapidly from orange-yellow to pink-red for Co(II) and red-orange or yellow for Zn(II). The reaction mixture was then refluxed for 6-7 h for Co (**1**) or Zn (**2**) (with HL1) or stirred for 6-7 h for Co (**3**) (with HL2) or refluxed for 15-16 h for Zn (**4**) (with HL2) and a precipitate was formed. Afterwards, the volume of the solvent was reduced to *ca.* 50% using a vacuum rotary evaporator until precipitation completed. The precipitate was then filtered off, washed 3 times with methanol (2 mL in each) and dried in air. The dried products were again dissolved in dichloromethane (DCM) and filtered. The filtrate was collected, the solvent was removed on a vacuum rotary evaporator and dried in air for 2-3 days to obtain pink-red (**1, 3**) or red-orange (**2**) or bright-yellow (**4**) microcrystals of bis[1-((X-phenylimino)methyl)naphthalen-2-olato-k^2N,O]cobalt or zinc(II) {X = 2-ethyl: Co (**1**) and Zn (**2**) or X = 4-methyl: Co (**3**) and Zn (**4**)}. Single crystals suitable for X-ray diffraction were grown by slow diffusion of n-hexane into a concentrated chloroform solution of **1** or slow diffusion of methanol into a concentrated dichloromethane solution of **3** or **4** after 2-3 days at room temperature. The syntheses of the Schiff bases, 1-((X-phenylimino) methyl)naphthalen-2-ol {X = 2-ethyl (HL1) or 4-methyl (HL2)} were reported in our previous communication [36,37].

2.2.1. Bis[1-((2-ethylphenylimino)methyl)naphthalen-2-olato-κ^{2}N,O] cobalt(II), (1)

Yield 360 mg (59%). – IR (KBr, cm^{-1}): 3039w, 2962w, 2927w, 2870w (C−H), 1616vs, 1602vs (C=N) and 1570vs (C=C). – MS (EI): *m/z* (%) = 607 (30) $[M = Co(L1)_2]^+$, 334 (45) $[Co(HL1)]^+$, 275 (100) $[HL1]^+$, 258 (22) $[L1-OH]^+$, 230 (35) $[C_{11}H_8NOCo+H]^+$, 132 (30) $[C_9H_{10}N]^+$ and 106 (37) $[C_7H_8N]^+$ {M = $[Co(L1)_2] = C_{38}H_{32}CoN_2O_2$ and HL1 = $C_{19}H_{17}NO$}. Conductance: $\Lambda_m = 3.33$ S m^2 mol^{-1} in DMF at 25 °C. Solid-state magnetic moment: $\mu_{eff.} = 4.16$ μB μB at 25 °C.

2.2.2. Bis[1-((2-ethylphenylimino)methyl)naphthalen-2-olato-κ^{2}N,O]zinc (II), (2)

Yield 380 mg (62%). – IR (KBr, cm^{-1}): 3064w, 3012w, 2962w, 2929w, 2870w (C−H), 1616vs, 1585vs (C=N) and 1570vs. ^{1}H NMR (400 MHz, $CDCl_3$): ∂/ppm = 1.15 (t, J_{HH} = 7.2 Hz, 3H, CH_3), 2.55-2.65 (m, 2H, CH_2), 6.57 (d, J_{HH} = 2.0 Hz, 1H, H_{14}), 6.67 (d, J_{HH} = 5.6 Hz, 1H, H_{17}), 7.10 (t, J_{HH} = 6.4 Hz, 1H, H_{15}), 7.17 (t, J_{HH} = 8.0 Hz, 1H, H_{16}), 7.40 (d, J_{HH} = 6.8 Hz, 1H, H_2), 7.71 (t, J_{HH} = 7.2 Hz, 1H, H_6), 7.72 (d, J_{HH} = 7.2 Hz, 1H, H_8), 7.82 (t, J_{HH} = 7.2 Hz, 1H, H_7), 7.83 (d, J_{HH} = 7.6 Hz, 1H, H_5), 8.25 (d, J_{HH} = 7.6 Hz, 1H, H_3) and 8.62 (d, J_{HH} = 6.8 Hz, 1H, CHN) (for hydrogen atom numbering see Fig. 1a). MS (EI): *m/z* (%) = 615 (5) $[\{M = Zn(L1)_2\} + H_2 + H]^+$, 277 (85) $[HL1+H_2]^+$, 262 (100) $[HL1+H_2-CH_3]^+$, 245 (85) $[HL1-C_2H_6]^+$, 233 (55) $[C_{11}H_7NOZn]^+$ and 106 (58) ($[C_7H_8N]^+$) {M = $[Zn(L1)_2] = C_{38}H_{32}ZnN_2O_2$ and HL1 = $C_{19}H_{17}NO$}. Conductance: $\Lambda_m = 5.26$ S m^2 mol^{-1} in DMF at 25 °C.

2.2.3. Bis[1-((4-methylphenylimino)methyl)naphthalen-2-olato-κ^{2}N,O] cobalt(II), (3)

Yield 350 mg (60%). – IR (KBr, cm^{-1}): 3055w, 3030w, 2980w, 2914w (C-H), 1614vs, 1598vs (C=N) and 1568vs. MS (EI): *m/z* (%) = 579 (35) $[M = Co(L2)_2]^+$, 319 (3) $[Co(HL2)]^+$, 260 (100) $[HL2-H]^+$, 244 (10) $[HL2-OH]^+$ and 91 (10) $[C_6H_5(CH_3)-H]^+$ {M = $[Co(L2)_2] = C_{36}H_{28}CoN_2O_2$ and HL2 = $C_{18}H_{15}NO$}. Conductance: $\Lambda_m = 0.45$ S m^2 mol^{-1} in DMF at 25°C. Solid-state magnetic moment: $\mu_{eff.} = 4.15$ μB at 25 °C.

2.2.4. Bis[1-((4-methylphenylimino)methyl)naphthalen-2-olato-κ^{2}N,O] zinc(II), (4)

Yield 440 mg (70%). – IR (KBr, cm^{-1}): 3057w, 3020w, 2920w, 2854w (C-H), 1616vs, 1598vs (C=N) and 1571vs (C=C). ^{1}H NMR (400 MHz, DMSO-d_6): ∂/ppm = 2.24 (s, 3H, CH_3), 6.96 (d, J_{HH} = 9.2 Hz, 1H, H_{17}), 7.15 (d, J_{HH} = 7.6 Hz, 2H, $H_{13,14}$), 7.25-7.32 (m, 3H, $H_{2,6,16}$), 7.50 (t, J_{HH} = 7.6 Hz, 1H, H_7), 7.77 (d, J_{HH} = 7.6 Hz, 1H, H_8), 7.90 (d, J_{HH} = 8.8 Hz, 1H, H_5), 8.31 (s, 1H, H_3) and 9.46 (s, 1H, CHN). (for hydrogen atom numbering see Fig. 1b). MS (EI): *m/z* (%) = 584 (5) $[M = Zn(L2)_2]^+$, 260 (100) $[HL2–H]^+$, 244 (12) $[[HL2–OH]]^+$ and 91

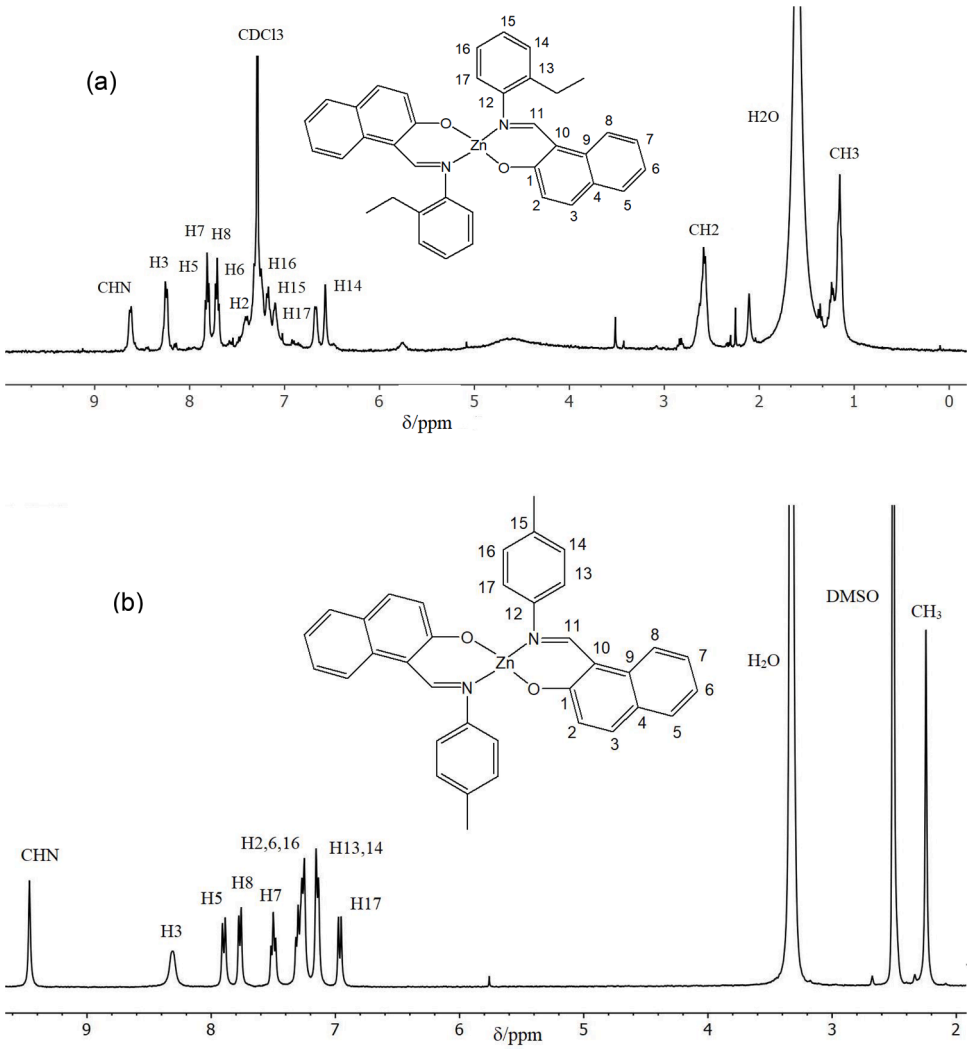

Fig. 1. ^{1}H NMR spectra for complex **2** in $CDCl_3$ (a) and **4** in DMSO-d_6 (b) at 20 °C.

(23) $[C_6H_5(CH_3)–H]^+$ {M = $[Zn(L2)_2] = C_{36}H_{28}ZnN_2O_2$ and HL2 = $C_{18}H_{15}NO$}. Conductance: $\Lambda_m = 0.39$ S m^2 mol^{-1} in DMF at 25 °C.

2.3. Decomplexation of compound 1 with NaCN

Complex **1** (ca. 5 mg) was dissolved in DMSO-d_6 in an NMR tube, and an excess amount of NaCN was added into this solution. The tube was carefully but thoroughly shaken to mix the solution well with the color changing from pink-red to red-orange. The ^{1}H NMR spectrum of this *in-situ* reaction mixture was ran at 20 °C (Fig. S4).

2.3.1. ^{1}H NMR data for in-situ reaction mixture of 1 and NaCN in DMSO-d_6

^{1}H NMR (400 MHz, DMSO-d_6): ∂/ppm = 1.17 (t, J_{HH} = 7.5 Hz, 3H, CH_3), 2.76 (q, J_{HH} = 7.5 Hz, 2H, CH_2), 6.61 (d, J_{HH} = 9.2 Hz, 1H, H_{14}), 6.87–6.91 (m, 2H, $H_{16,17}$), 6.97 (t, J_{HH} = 7.2 Hz, 1H, H_{15}), 7.14-7.22 (m, 3H, $H_{2,6,7}$), 7.39-7.42 (m, 2H, $H_{5,8}$), 9.19 (s, 1H, CHN) and 9.65 (d, J_{HH} = 8.4 Hz, 1H, H_3) (for hydrogen atom numbering see Fig. S4).

2.4. X-ray crystallography

Compound **1**: Suitable crystals were carefully selected under a polarized-light microscope, covered in protective oil and mounted on a cryo-loop. The single crystal diffraction data was collected using a Rigaku XtaLAB Synergy S four circle diffractometer with a Hybrid Pixel Array Detector and a PhotonJet X-ray source for Cu-Kα radiation (λ = 1.54184 Å) with a multilayer mirror monochromator. Data collection at 100.0 ± 0.1 K using ω-scans. Data reduction and absorption correction were performed with CrysAlisPro 1.171.41.105a [41], Structure analysis and refinement: The structures were solved by direct methods (SHELXT-2015). Full-matrix least-squares refinements on F^2 were carried out using the SHELXL-2017/1 program package in OLEX 2.1.3 [42–44]. A highly disordered solvent molecule was masked by using the solvent mask feature as implemented in the OLEX 2.1.3 [44]. All hydrogen atoms on C were positioned geometrically (with C–H = 0.95 Å for aromatic and aliphatic CH, C–H = 0.99 Å for CH_2 and C–H = 0.98 Å for CH_3) and refined using riding models (AFIX 43, 23 and 137 with $U_{iso(H)} = 1.2\ U_{eq}$ (CH, CH_2) and 1.5 U_{eq} (CH_3). Crystal data and details on the structure refinement are given in Table 1. Graphics were drawn with the program DIAMOND [45]. Computations on the supramolecular interactions were carried out with PLATON for Windows [46–49].

Compound **3** and **4**: X-ray crystal structure data were collected from multi-faceted crystals of suitable size and quality, selected from a representative sample of crystals of the same habit using an optical microscope. Crystals were mounted on MiTeGen loops and data collection was carried out in a cold stream of nitrogen (150 K; Bruker D8 QUEST ECO). Diffractometer manipulations were carried out using Bruker APEX4 software [50]. Structure solution and refinement were performed using XS, XT and XL software, embedded within the OLEX2

Table 1
Crystal data and structure refinement for compounds **1**, **3** and **4**.

Complexes	**1**	**3**	**4**
Empirical formula	$C_{38}H_{32}CoN_2O_2$	$C_{36}H_{28}CoN_2O_2$	$C_{36}H_{28}ZnN_2O_2$
M (g mol^{-1})	607.59	579.53	585.97
Crystal size (mm)	0.115 × 0.153 × 0.194	0.180 × 0.178 × 0.057	0.275 × 0.124 × 0.028
Temperature (K)	100	150	150
θ range (°)	2.82–67.05	4.85 - 52.74	4.86 - 50.17
h; k; l range	+37,−32; +36,−37; ±21	±12; ±13; ±18	±11; ±12; ±17
Crystal system	trigonal	triclinic	triclinic
Space group	R-3	P-1	P-1
a (Å)	31.396(1)	9.912(3)	9.917(2)
b (Å)	31.396(1)	10.747(4)	10.719(2)
c (Å)	17.695(1)	14.983(6)	14.994(4)
α (°)	90	86.44	77.59
β (°)	90	70.70	70.71
γ (°)	120	64.99	65.09
V (Å^3)	15,105.49(13)	1359.5(9)	1359.1(6)
Z/D (calc/g cm^{-3})	18/1.202	2/1.416	2/1.432
F(000)/μ (mm^{-1})	5706.0/4.265	602.0/0.669	608.0/0.941
Max/min transmission	0.955/0.955	0.745/0.698	0.745/0.673
Refl. measured	62,045	35,941	42,505
Refl. unique/R_{int}	5999/0.0262	5551/0.0274	4707/0.0330
Data/restraints/parameters	5999/0/390	5551/0/372	4707/0/373
Completeness	1.000	0.997	0.974
Largest diff. peak & hole (ρ /e $\AA^{-3}$)	0.202/−0.317	0.37/−0.41	1.69/−0.51
R_1/wR_2 [$I > 2\sigma(I)$] [a]	0.0328/0.0841	0.0327/0.0784	0.0661/0.1843
R_1/wR_2 (all reflect.) [a]	0.0336/0.0847	0.0378/0.0810	0.0690/0.1866
Goodness-of-fit on F^2 [b]	1.024	1.067	1.195
CCDC number	2,241,378	2,240,728	2,252,041

− [a] $R_1 = [\Sigma(||F_o|-|F_c||) / \Sigma |F_o|]$; $wR_2 = [\Sigma [w(F_o{}^2-F_c{}^2)^2]/\Sigma[w(F_o{}^2)^2]]^{1/2}$. − [b] Goodness-of-fit = $[\Sigma [w(F_o{}^2-F_c^2)^2] /(n-p)]^{1/2}$.

[44]. For each structure, the absence of additional symmetry was confirmed using ADDSYM incorporated in the PLATON program [46–49]. Crystal data and details on the structure refinement are given in Table 1. The CCDC numbers are 2241378 (**1**) and 2240728 (**3**) and 2252041 (**4**), and contain the supplementary crystallographic data reported in this paper. These data can be obtained free of charge from the Cambridge Crystallographic Data center *via* www.ccdc.cam.ac.uk/data_request/cif.

2.5. Powder X-ray diffraction (PXRD) studies

Powder X-ray diffraction (PXRD) data were recorded on GNR Explorer powder X-ray diffractometer operating in the Bragg-Brentano geometry with Cu-Ka radiation (l = 1.5406 Å) at 40 kV and 30 mA using zero background silicon sample holder. Data were collected with a 2θ step size of 0.02 ° and an integration time of 3.0 s over an angular range of 5–45 ° (2θ) at 25 °C. The PXRD patterns for complexes **1** and **3** were indexed using two different indexing programs (N-Treor09 [51] and DICVOL [52]) implemented in Expo2014 software [53]. For indexing of the experimental diffractogram, we used most intense low angle peaks selected from 5 to 30 ° (2θ) (18 peaks for **1** and 22 peaks for **3**), assuming a trigonal crystal system for **1** and a triclinic one for **3**. The most probable solutions were obtained by considering figure of merit (M20) and visually comparing calculated peaks positions and experimental peaks. The indexed cell parameters are listed in Table 2. The indexing of the simulated diffractograms is given as Tables S3 (**1**) and S4 (**3**).

Table 2
Indexed cell parameters from experimental PXRD patterns for **1** and **3**.

Parameters	Complex **1**	Complex **3**
Crystal system	trigonal	triclinic
a (Å)	31.732	9.912
b (Å)	31.732	10.749
c (Å)	17.474	14.986
α	90.00	86.43
β	90.00	70.73
γ (°)	120.00	64.98
V (Å^3)	15,237.83	1360.23

2.6. Computational method

Computational procedure was executed with the Gaussian 09 software [54]. For computation, the initial geometries for cobalt(II) complexes (**1** and **3**) were generated from the X-ray structures. The geometry optimization by density functional theory (DFT) was performed at B3LYP/6-31G(d). The excited state properties (UV–Vis. spectra) were calculated by time-dependent density functional theory (TD-DFT) with different combinations of the functionals B3LYP and M06 and the basis sets 6-31G(d), DEF2SVP, SDD, SVP and TZVP, respectively (Fig. S6a-b). The PCM (polarization continuum model) in chloroform and 72 excited states were considered for calculations (Tables S5 and S6). Molecular orbitals (MOs) calculations for spectral assignments were executed at the same level of theory. The simulated electronic spectra were shaped with SpecDis (version 1.71) [55], applying Gaussian band shape with an exponential half-width of σ = 0.16 eV.

3. Results and discussion

The Schiff bases 1-((X-phenylimino)methyl)naphthalen-2-ol {X = 2-ethyl (HL1) or 4-methyl (HL2)} react with cobalt(II) or zinc(II) acetate to give the bis[1-((X-phenylimino)methyl)naphthalen-2-olato-k^2N,O]cobalt(II) or zinc(II) complexes {X = 2-ethyl: M = Co (**1**) and Zn (**2**) or X = 4-methyl: M = Co (**3**) and Co (**4**)} (Scheme 1). Vibrational spectra showed very strong bands at ca. 1616, 1600, 1598 cm^{-1} for νC=N and ca. 1578, 1568 cm^{-1} for νC=C (Fig. S1) [9–12,16–24]. Electron impact (EI) mass spectra exhibited the parent ion peak at m/z = 607 (**1**), 615 (**2**), 579 (**3**) and 584 (**4**) with several ions peaks for the fragmented Schiff bases and complexes (see experimental section and Fig. S2a-d). The very low molar conductance Λ_m = 3.33 (**1**), 5.26 (**2**), 0.45 (**3**) and 0.39 S m^2 mol^{-1} (**4**) indicates non-electrolyte nature of the complexes in DMF at 25 °C.

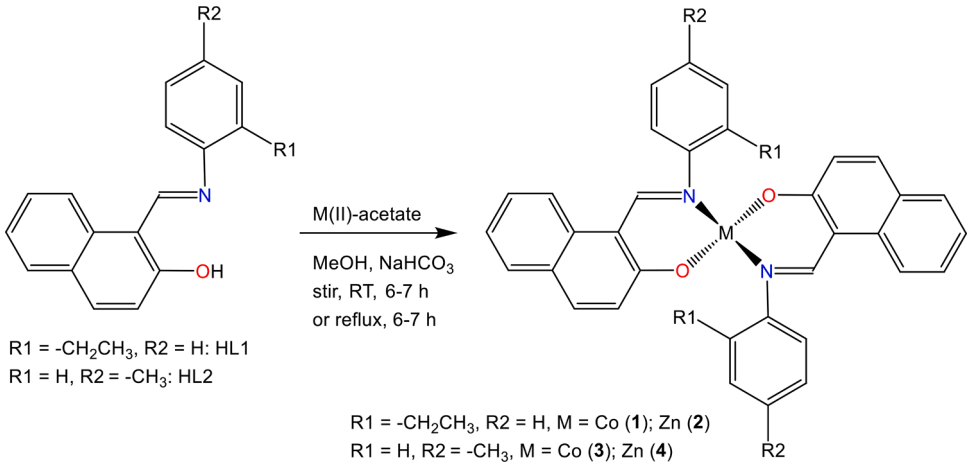

Scheme 1. Synthetic route to the formation of bis[1-((X-phenylimino)methyl)naphthalen-2-olato-κ^{2}N,O]cobalt(II) and zinc(II) complexes (**1–4**).

3.1. ^{1}H NMR studies

The ^{1}H NMR spectra for **2** and **4** (Fig. 1) are dominated by several peaks mainly for the coordinated Schiff base ligands to the zinc(II) ion. The spectrum for **2** (Fig. 1a) shows a triplet at δ = 1.15 ppm (J_{HH} = 7.2 Hz) and a multiplet at δ = 2.55–2.65 ppm for the methyl and methylene protons, respectively [36]. The spectrum for **4** (Fig. 1b) shows a singlet at δ = 2.24 ppm for the methyl protons. The imine proton peak is shifted to high field upon coordination of the nitrogen atom (from ligand) to the metal ion and appeared as a doublet at δ = 8.62 ppm (J_{HH} = 6.8 Hz) for **2** (9.34 ppm in HL1 [36]), while a singlet at δ = 9.46 ppm for **4** (9.61 ppm in HL2 [37]). The absence of any phenolic proton peak (usually observed as a broad peak at δ = 15.63 ppm in HL1 and 15.90 ppm in HL2) indicates coordination of the ligands to the metal ion and subsequent formation of a bond between the O^- and Zn^{2+} ions. Indeed, several aromatic protons (Ar-H) peaks are observed in the range of δ = 6.57–8.31 ppm (see experimental section and Fig. 1 for detailed peak assignments).

The ^{1}H NMR spectra for **1** and **3** in $CDCl_3$ (Fig. S3a-b) displayed peak broadening and shifting effects, suggesting paramagnetic nature of the cobalt(II) complexes [17,21]. When complex **1** is reacted with NaCN in DMSO-d_6 the octahedral diamagnetic $[Co^{III}(CN)_6]^{3-}$ species forms with release of the deprotonated Schiff base in solution, as evidenced by the ^{1}H NMR spectrum (see Fig. S4 and the data in experimental section under 2.3). The reaction is accompanied by a color change from pink-red to red-orange. The ^{1}H NMR spectrum of *in-situ* reaction mixture of **1** and NaCN in DMSO-d_6 (see Fig. S4) then corresponds well to the deprotonated Schiff base ligand [36]. The solid-state magnetic moment values $\mu_{eff.}$ = 4.16 (**1**) and 4.15 (**3**) μ_B at 25 °C (without diamagnetic correction for the ligands) agree well with the paramagnetic nature of tetrahedral cobalt(II)-d^7 complexes with an e^4d^3 configuration with three unpaired electrons. Similar magnetic moment values are reported for the analogous Co(II)-N,O-chelate Schiff base complexes in solution and solid-state (ca. 4.20 μ_B) [21]. The theoretical spin-only magnetic moment for three unpaired electrons (S = 3/2) is $\mu_{eff.}$ = 3.87 μ_B, with spin-orbit coupling the value is $\mu_{eff.}$ = 5.20 μ_B [21,56].

3.2. Electronic and simulated spectra

Electronic spectra for the Schiff base (HL) and complexes (**1**, **3** and **4**) were measured in chloroform at 25 °C (Figs. 2, 3, S5 and Table 3). The spectral patterns for the complexes are almost similar with little differences from the Schiff base, in particular in the visible region. The spectra feature several bands/shoulders below 500 nm due to the ligand-centered n→π*/π→π* (LL) electrons transitions [17–18,20,21]. Furthermore, spectra for the Co(II) complexes (**1** and **3**) display a weak broad band/shoulder in the visible region (500-650 nm) which arise from metal-centered d-d (MM) electrons transitions, which is obviously absent in HL, **2** and **4** (Figs. 2, 3, S5; inset) [17,21].

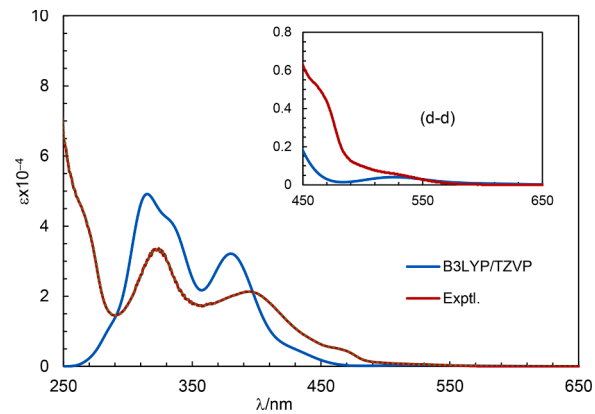

Fig. 2. Electronic and simulated spectra for **1** (ca. 0.028 mM) in chloroform at 25 °C. Spectra at visible range are shown in inset. Simulated spectrum at B3LYP/TZVP with PCM in chloroform. Gaussian band shape with exponential half-width of σ = 0.16 eV.

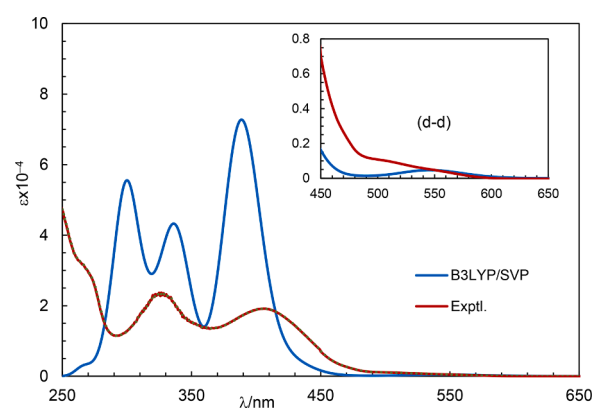

Fig. 3. Electronic and simulated spectra for **3** (ca. 0.022 mM) in chloroform at 25 °C. Spectra at visible range are shown in inset. Simulated spectrum at B3LYP/SVP with PCM in chloroform. Gaussian band shape with exponential half-width of σ = 0.16 eV.

Excited state properties for Co(II) complexes (**1** and **3**) by TD-DFT were calculated with different combinations of the functional (e.g., B3LYP and M06) and the basis sets (e.g., 6–31G(d), SVP, TZVP and

Table 3
Selected excitation properties for **1** and **3**, calculated at B3LYP/TZVP and B3LYP/SVP with PCM in chloroform, respectively.[#]

λ/nm[1]	Excited state	Oscillator strength (f)	MO contribution (%)[2]	Assignments[3]
			Compound **1**	
527 (530 sh)	7	0.0026	H-1→L (42), H→L+1 (27)	MM, LM/LM, LL
424 (465 sh)	10	0.0294	H-1→L (44), H-1→L+1 (36)	MM, ML, LL
392 (395)	13	0.1058	H→L (74), H→L+2 (24)	LM, LL
339	25	0.1769	H-7→L (11), H-2→L (46)	LM, LL
320 (324)	32	0.1344	H-1→L+3 (71), H-1→L+6 (15)	MM, ML, LL
309 (279 sh)	38	0.1310	H→L+4 (67)	LM, LL
			Compound **3**	
549 (515 sh)	7	0.0036	H-1→L (49), H→L+1 (51)	MM, LM/LM, LL
431 (435 sh)	12	0.0311	H-4→L+1 (27), H-2→L (43)	LM, LL
394 (406)	14	0.3010	H-1→L (94)	MM, ML, LL
345	26	0.1820	H-3→L (31), H-2→L (36)	LM, LL
316 (325)	35	0.3448	H-1→L+3 (25), H→L+4 (35)	ML/LM, LL
296 (273 sh)	48	0.1003	H-1→L+6 (30), H→L+5 (55)	MM, ML/LM, LL

[#] Molecular orbitals (MOs) for β-spin electrons consideration.
[1] Experimental values are in parentheses.
[2] H/*L*= HOMO/LUMO.
[3] MM = metal-metal, ML/LM = metal-ligand/ligand-metal and LL= ligand-ligand electrons transitions.

SDD), respectively (Fig. S6a-b). The simulated spectra (UV–vis.) thus obtained from different methods are almost identical with little shifting of the bands' maxima and are comparable with the experimental spectra (Fig. S6a-b). Indeed, the best matching of simulated and experimental spectra is observed with B3LYP/TZVP (**1**) or B3LYP/SVP (**3**) calculations (Figs. 2, 3). Some selected and simplified assignments on simulated spectra were made based on orbital and population analysis [17,21], and data are listed in Table 3 along with the experimental data. The simulated spectra display a weak broad band in the visible region, very similar to the experimental spectra (Figs. 2, 3; inset). The band found at ca. 527 (**1**) or 549 (**3**) nm arises from combinations of MM, ML/LM and LL electrons excitations from HOMO−1 to LUMO transitions (Fig. 4) with molecular orbitals (MOs) contributions of 42 (**1**) or 49% (**3**). However, the most populated and significant band is observed at ca. 392 (**1**) or 394 (**3**) nm with the highest MOs contributions of 74% from HOMO to LUMO (**1**) or 94% from HOMO-1 to LUMO (**3**) transitions (Table 3).

3.3. X-ray molecular and optimized structures

X-ray molecular structure determinations for **1, 3** and **4** reveal that two molecules of the N,O Schiff base ligands chelate the metal ion to form a pseudotetrahedral N_2O_2-coordination sphere around the metal (II) atom (Fig. 5, left). Two unsymmetrical chiral N,O-chelate ligands in tetrahedral geometry induce the formation of metal-centered Λ/Δ-chirality along the C_2-symmetry of the molecule, diastereoselectively provide two diastereomers Δ-M(*R*-N,O)$_2$ and Λ-M(*R*-N,O)$_2$ {or Λ-M(*S*-N,O)$_2$ and Δ-M(*S*-N,O)$_2$} with one being thermodynamically favoured [16–25,27–32]. In the absence of a chiral ligand there is, however, no diastereomeric induction and in the centrosymmetric space groups R–3 (**1**) and P–1 (**3** or **4**) there is an equal amount of Λ- and Δ-chiral complexes, hence a racemic mixture of two stereoisomers. Compound **3** and **4** are isostructural. The bond lengths and angles are listed in Table 4, comparable to analogous pseudotetrahedral Co/Zn (II)-N,O-chelate Schiff base complexes [17,18,20,21,25,34,35]. Inspection of metal-ligand bonds lengths in the six-membered chelate ring shows that the M–O bond is shorter than the M–N bond, which suggests

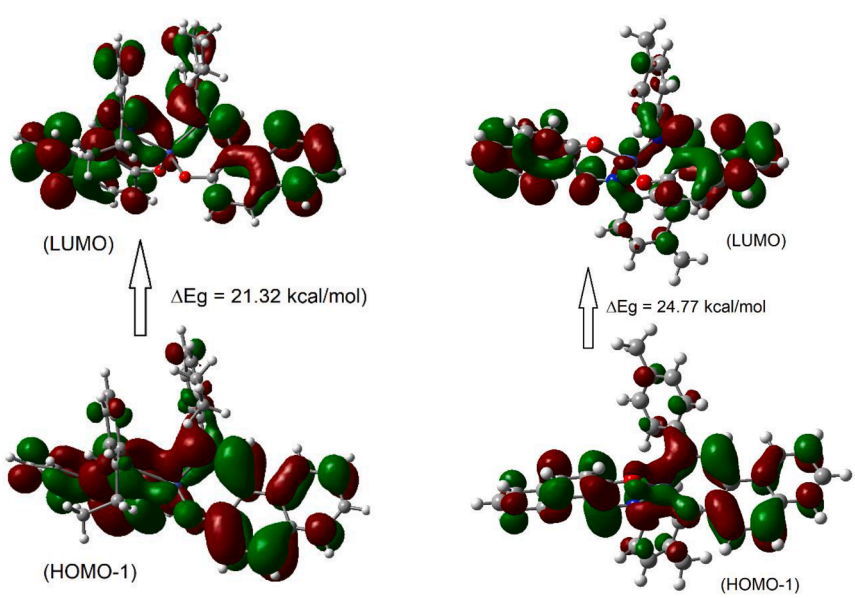

Fig. 4. The MOs for HOMO-1 and LUMO for **1** (left) and **3** (right) (for β-spin electrons consideration).

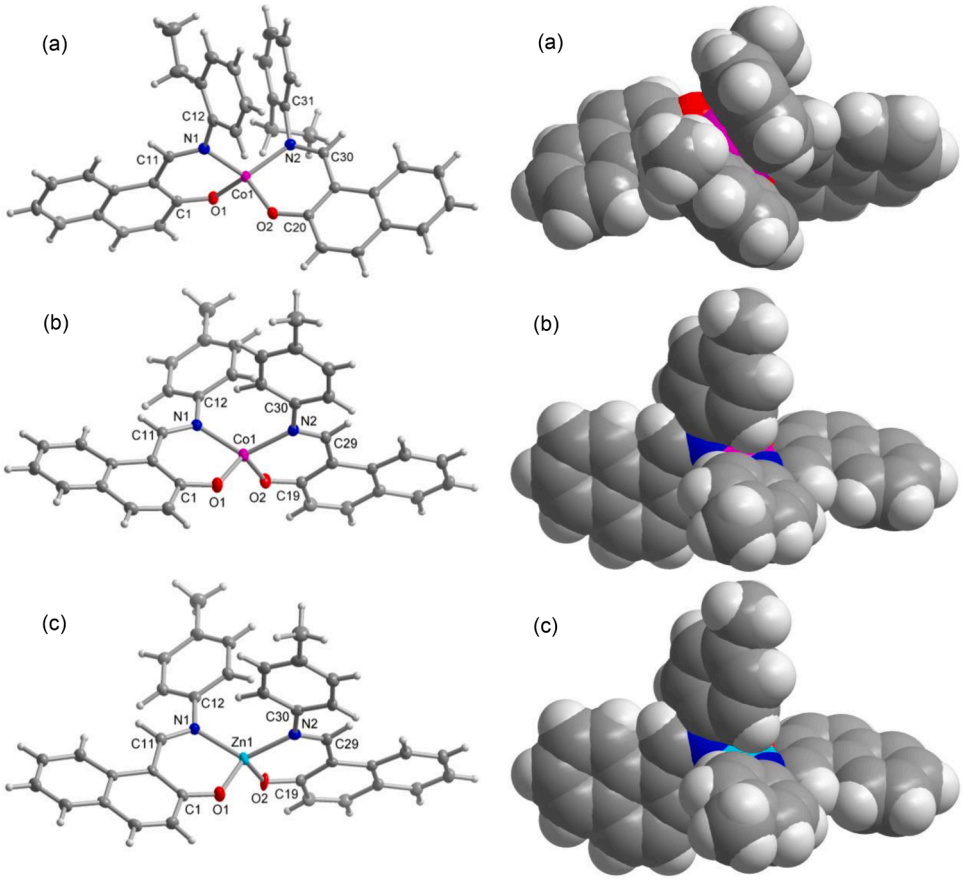

Fig. 5. Molecular structures of **1** (a), **3** (b) and **4** (c) {50% thermal ellipsoids; H atoms with arbitrary radii (left) and in space-filling mode (right)}. See figure S8 for structures with full atom labeling.

Table 4
Selected bond lengths (Å) and angles (°) in **1, 3** and **4**.

Bond lengths (Å)/ angles (°)	X-ray structure **1** (M = Co)	Opt. structure **1** (M = Co)	Bond lengths/ angles	X-ray structure **3** (M = Co)	Opt. structure **3** (M = Co)	X-ray structure **4** (*M* = Zn)	Opt. structure **4** (*M* = Zn)
Co1-O1/ Co1-O2	1.913(1)/1.905(2)	1.9079/1.9066	M-O1/ M-O2	1.904(2)/1.908(2)	1.9061/1.9061	1.917(6)/1.942(5)	1.9312/1.9314
Co1-N1/Co2-N2	1.984(2)/1.986(1)	1.9781/1.9873	M-N1/M-N2	1.988(2)/1.992(2)	1.9826/1.9827	2.001(6)/1.996(7)	2.0088/2.0087
C1-O1/C20-O2	1.303(2)/1.308(3)	1.2971/1.2956	C1-O1/C19-O2	1.302(3)/1.297(3)	1.2933/1.2933	1.30(1)/1.31(1)	1.3204/1.3204
C12-N1/C31-N2	1.433(2)/1.437(3)	1.4334/1.4329	C12-N1/C30-N2	1.435(3)/1.434(2)	1.4231/1.4232	1.431(8)/1.428(7)	1.4380/1.4380
C11-N1/C30-N2	1.305(3)/1.309(3)	1.3142/1.3169	C11-N1/C29-N2	1.311(3)/1.310(3)	1.3191/1.3191	1.30(1)/1.31(1)	1.3328/1.3327
O1-Co1-N1/O2-Co1-N2	92.42(6)/93.19(6)	93.61/94.17	O1-M-N1/O2-M-N2	94.51(7)/94.68(6)	94.26/94.27	94.90(2)/95.60(2)	93.98/93.97
O1-Co1-O2/N1-Co1-N2	112.87(6)/111.75(7)	115.52/117.93	O1-M-O2/N1-M-N2	118.80(6)/123.22(7)	116.82/124.46	116.60(2)/124.80(2)	119.37/124.15
O1-Co1-N2/O2-Co1-N1	128.99(6)/120.30(6)	121.78/115.71	O1-M-N2/O2-M-N1	117.11(7)/110.34(6)	114.46/114.42	116.80(2)/109.50(2)	113.84/113.76
$\theta/\tau_{tet\text{-}sq}/\tau_4$	79.99/0.89/0.79	88.46/0.98/0.85	$\theta/\tau_{tet\text{-}sq}/\tau_4$	83.90/0.93/0.84	85.14/0.95/0.84	83.95/0.93/0.84	83.51/0.93/0.83

stronger bonding interaction between the O^- and M^{2+} ions (Table 4). Furthermore, the metal-ligand bond lengths (M–O/N) are slightly longer for Zn(II) complex (**4**) than those for Co(II) complexes (**1** and **3**) due to larger size of the zinc atom (covalent radii Co 1.16 Å, Zn 1.25 Å) (Table 4). It is noteworthy that as we go from **1** to **3** or **4**, both the O1–M–O2 and N1–M–N2 bond angles increase, with the N1–M–N2 angle increasing to a much greater extent. O1–M–O2 goes from 112.9° in **1** to 118.8° in **3** or 116.6° in **4**, whereas N1–M–N2 goes from 111.8° in **1** to 123.2° in **3** or 124.8° in **4**. This is a result of the steric repulsion between the N-bound phenyl rings. The 2-ethyl-phenyl rings in **1** rotate out of the plane of the chelate ring and enter into a π-π orientation (Fig. 5a, right), which allows a close approach. In isostructural **3** or **4**, we see that the 4-methyl-phenyl ring is more planar with the chelate ring and the two phenyl rings assume a C–H–π orientation (Fig. 5b-c, right), which however pushes the N1–Co1–N2 further apart due to the steric larger distance between the two phenyl rings. The interplanar phenyl-chelate ring angles are 57.5° and 67.3° in **1**, 33.6° and 24.8° in **3** or 31.8° and 23.3° in **4**. The optimized structures for **1, 3** and **4** are shown in Fig. S7, and the bond lengths and angles, which are also listed in Table 3, are similar to the experimental data.

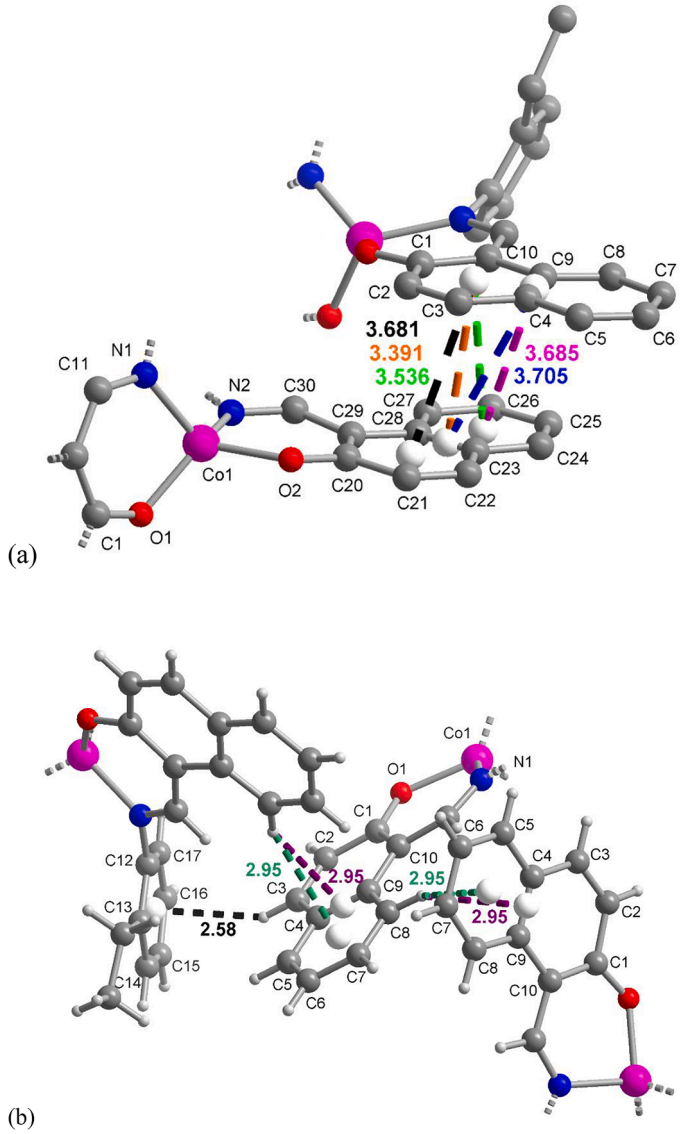

Fig. 6. Significant intermolecular π–π (a) and C-H-π (b) interactions between the neighbouring molecules in the naphthyl rings in compound **1**. The centroid-centroid distances in (a) and the H-centroid distances in (b) are given in Å.

Inspection of the O/N-M-O/N bond angles around Co in **1** and **3** or Zn in **4** shows a deviation by up to 20 ° from a tetrahedral configuration around the metal atom. The degree of distortion from tetrahedral can be expressed by the dihedral angle ($\theta/°$) between the two planes formed by the donor atoms with the metal atom (i.e., N1-Co-O1 and N2-Co-O2) [16–18,20–25,57]. This can also be estimated by a normalized function of the dihedral angle ($\tau_{\text{tet-sq}} = \theta/90°$) or by the tetrahedral geometry index ($\tau_4 = \{360° - (\alpha + \beta)\}/141°$, where α and β are the two largest angles in the four-coordinate species) [58]. The values of θ, $\tau_{\text{tet-sq}}$ and τ_4 are listed in Table 4 and the parameters $\tau_{\text{tet-sq}}$ and τ_4 are in good accord with each other.

Supramolecular packing analyses by PLATON [46] for compound **1** indicate significant intermolecular π–π and C-H−π interactions between the neighbouring molecules in the naphthyl rings (Fig. 6 and Tables S1 and S2) [59–64]. All listed π−π and C-H−π interactions are illustrated as dashed lines with the centroid-centroid contacts and C-H-centroid contacts, respectively in Fig. 6.

3.4. Powder X-ray diffraction (PXRD)

Powder X-ray diffraction (PXRD) patterns for **1** and **3** were measured over the 2θ range of 5–45 ° at ambient temperature (Fig. 7). Fair matching of respective experimental and simulated patterns from single crystal X-ray structure confirms the phase purity of microcrystalline bulk sample (Fig. 7). A very small shift in peak positions between simulated and experimental patterns for **3** is usually due to sample preparation, different temperature, etc. Complex **1** and complex **3** however have to give a different pattern in view of their different crystal system, space group and molecular packing (Table 1). The indexed cell parameters were obtained from experimental PXRD pattern (Table 2) and are very similar with the single crystal X-ray data (Table 1). Complex **1** crystallizes in the trigonal crystal system, while complex **3** in the triclinic one. The indexed simulated diffractograms are provided as Tables S3 (**1**) and (**3**) in the Supp. Info.

3.5. Thermal analysis

Thermal analysis for compounds **1**, **3** and **4** by differential scanning calorimetry (DSC) yielded the phase transformation temperature and enthalpy changes (ΔH) (Fig. 8 and Table 5) [17–25,37]. The DSC heating curve shows an endothermic peak at ca. 162 °C (**1**) and 253 °C (**3**) with an enthalpy change of $H = -20.57$ (**1**) and -47.16 (**3**) kJ mol^{-1}, corresponds to phase transformation from microcrystals (Cr) to isotropic-liquid (I or m. p.) (i.e., Cr ⇆ I). The heating curve for **4** shows two endothermic peaks at ca. 173 °C (ΔH = −12.45) and 250 °C (ΔH = −42.69), corresponds to phase transformation from microcrystals (Cr) to solid-crystals (Cr ⇆ SCr) and then to isotropic-liquid (i.e., SCr ⇆ I), respectively. The cooling curve shows no corresponding peak on the reverse direction except a very weak peak at ca. 71 °C (**1**), 85 °C (**3**) and 88 °C (**4**) for glass transition temperature (Tg). The heating curve for the same sample (probe) in the second cycle reproduces almost similar results (except for **1**) with an extra peak for Tg at ca. 89 °C (**1**), 110 °C (**3**) and 105 °C (**4**) (Table 5). Thermal analysis suggests an irreversible phase transformation and subsequent thermal stability for the complexes. However, optical observations by polarizing light microscopic (PLM) using a heating-cooling stage show no mesomorphic property for these complexes, alike the homoleptic square-planar copper(II) complex [37].

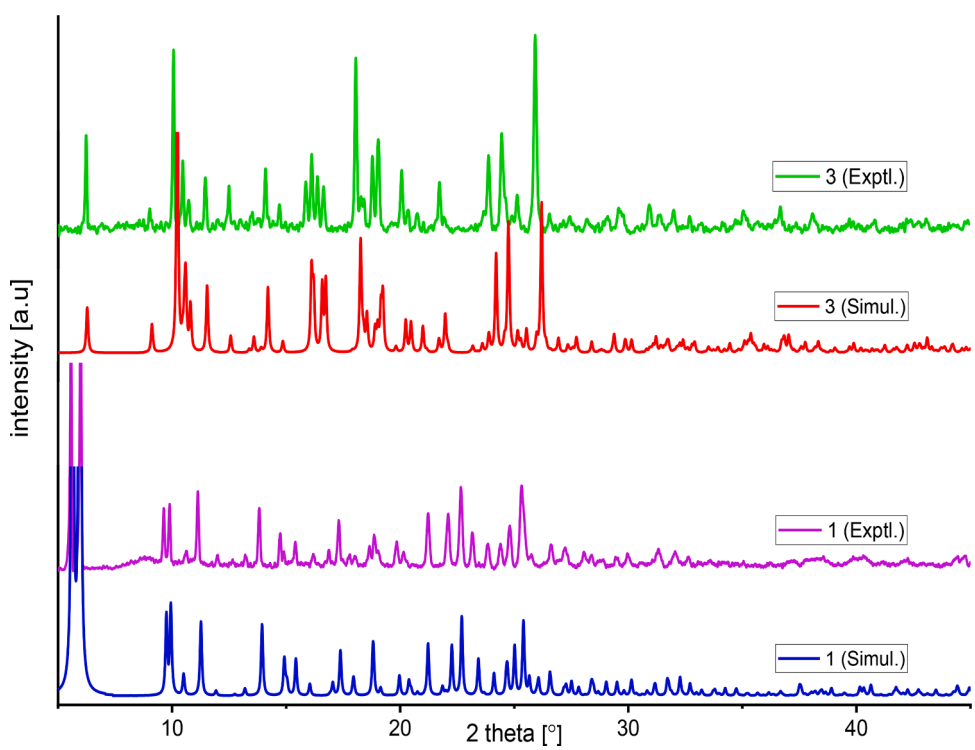

Fig. 7. Experimental (at ambient temperature) and simulated PXRD plots (from low temperature crystal structure determination) for **1** and **3**.

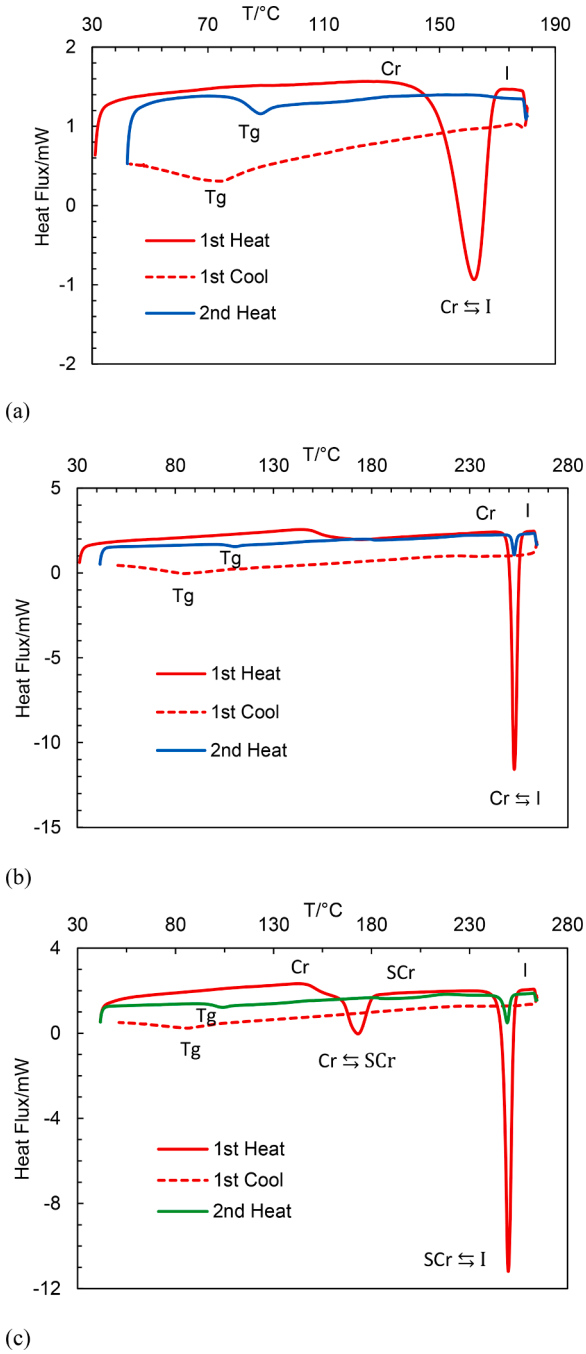

Fig. 8. Differential scanning calorimetry (DSC) heating curve for **1** (a), **3** (b) and **4** (c) (Cr = Microcrystals, SCr = Solid-crystals, I = Isotropic-liquid (m.p.), Tg = Glass transition temperature).

3.6. Cyclic voltammetry

Cyclic voltammograms for cobalt complexes **1** and **3** were recorded at a range of −1.80 to 1.20 V vs. Ag/AgCl at varying scan rates (ν/V s^{-1}) in N,N-dimethylformamide (DMF) at 25 °C (Fig. 9). The reductive wave, at a scan rate of 0.10 V/s, displays a strong broad cathodic peak centered at ca. −1.24 V (Ic = +14.40 μA) for **1** and −0.85 V (Ic = +12.63 μA) for **3**, suggests two one electron charge transfer processes for $[Co(L)_2]/[Co(L)_2]^-$ (Co^{2+}/Co^+) and $[Co(L)_2]^-/[Co(L)_2]^{2-}$ (Co^+/Co^0) couples (L = deprotonated Schiff base). On the other hand, the oxidative wave

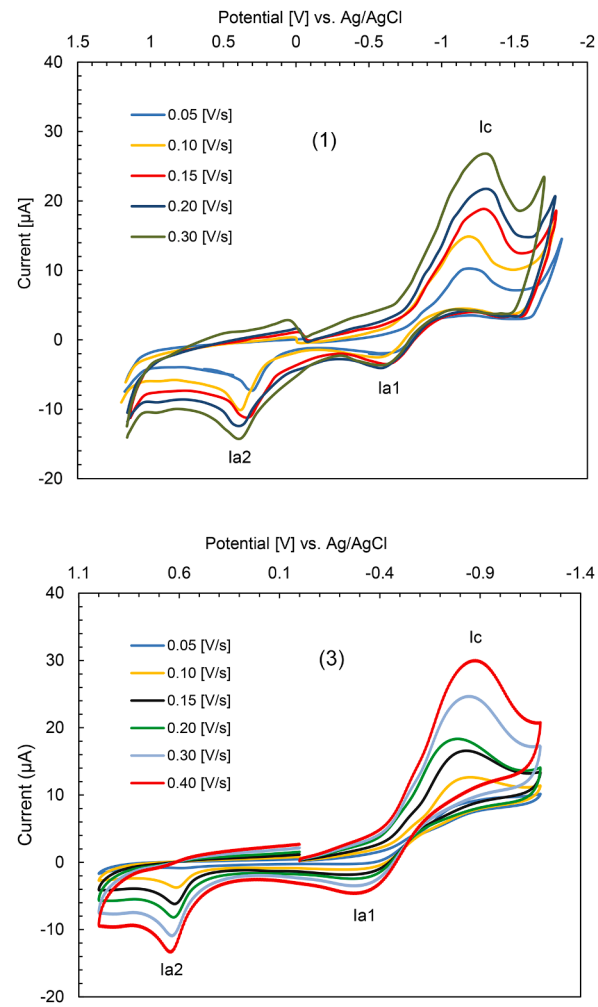

Fig. 9. Cyclic voltammograms for **1** (ca. 0.5 mM) and **3** (ca. 0.5 mM) at varying scan rates (ν [V/s]); TBAP (ca. 0.1 M) in N,N-dimethylformamide (DMF) at 25 °C.

Table 5
Phase transformation temperature and enthalpy change (ΔH) for **1, 3** and **4**.

Compounds	Cycles	$T^{\#}$ (°C)/ΔH* (kJ mol^{-1}) (heating curve)	$T^{\#}$ (°C)/ΔH* (kJ mol^{-1}) (cooling curve)
1	1st cycle	162/−20.57 (Cr ⇆ I)	71 (Tg)
	2nd cycle	89 (Tg)	–
3	1st cycle	253/−47.16 (Cr ⇆ I)	85 (Tg)
	2nd cycle	110 (Tg), 253/−2.75 (Cr ⇆ I)	–
4	1st cycle	173/−12.45 (Cr ⇆ SCr),250/−42.69 (Cr ⇆ I)	88 (Tg)
	2nd cycle	105 (Tg), 249/−3.56 (Cr ⇆ I)	–

#Peak temperature; *Enthalpy change or heat of transformation.
Cr = Microcrystals, SCr = Solid-crystals, I = Isotropic-liquid (m. p.), Tg = Glass transition temperature.

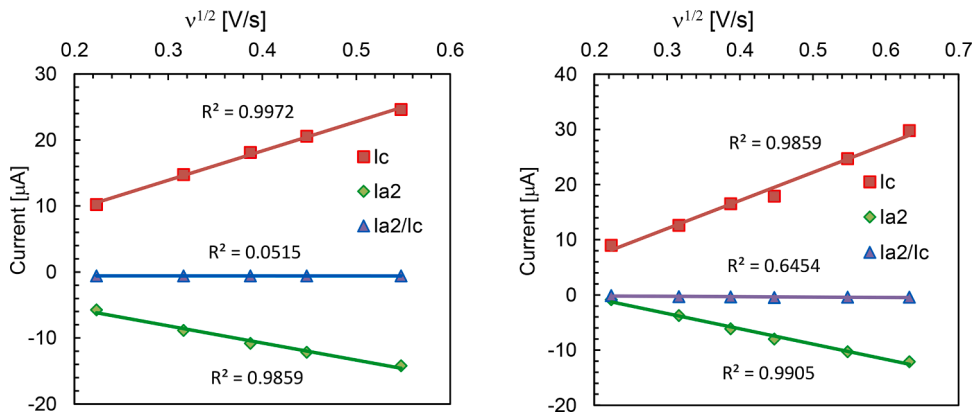

Fig. 10. Plot of peak current (Ic or Ia2 or Ia2/Ic [μA]) vs. $\nu^{1/2}$ [V/s] for **1** (left) and **3** (right) in N,N-dimethylformamide (DMF) at 25 °C.

shows two well separated anodic peaks centered at ca. −0.60 V (Ia1 = −3.65 μA) and +0.39 V (Ia2 = −10.78 μA) for **1** and ca. −0.38 V (Ia1 = −1.73 μA) and +0.63 V (Ia2 = −3.69 μA) for **3**, corresponds to two one electron charge transfer processes for Co^0/Co^+ and Co^+/Co^{2+} couples, respectively. The CV patterns recorded at varying scan rates reveal that the cathodic and anodic peaks shift to lower and higher potential, respectively with faster scan rate. The plot of peak current (Ic or Ia2 or Ia2/Ic) vs. square root of the scan rate ($\nu^{1/2}$) shows an increase of cathodic peak current (Ic) or a decrease of anodic peak current (Ia), while the ratio of Ia2/Ic remains unchanged with faster scan rates (Fig. 10). The linear plot suggests a diffusion-controlled electrochemical process in solution. The CV results suggest a quasi-reversible two one electron charge transfer processes in solution, reported for the analogous metal(II)-N,O-chelate Schiff bases complexes [19,21,23,24,26,37].

4. Conclusions

Molecular structure determinations for the titled compounds bis[1-((X-phenylimino)methyl)naphthalen-2-olato-k^2N,O]cobalt(II) and zinc (II) (**1** - **4**) showed that two molecules of the N,O-chelate ligands form a N_2O_2-chromophore around the metal ion in a pseudotetrahedral geometry. Coordination of two asymmetrical N,O-chelates induced Λ/Δ-chirality at the metal atom along the C_2-symmetry of the molecule albeit as a racemic mixture of Λ/Δ-Co/Zn(N,O) stereoisomers in the absence of any ligand chirality. Changes of substituents and their positions on the N-bound phenyl ring in the coordinated Schiff bases ligands resulted in a geometrical change around the metal atom. The phase purity of bulk microcrystalline sample was confirmed by fair matching of the experimental and simulated PXRD patterns. Thermal analysis suggests an irreversible phase transformation from solid crystals to isotropic-liquids and thermal stability of the complexes. Electrochemical analysis designates a quasi-reversible two one electron charge transfer processes for **1** or **3** in DMF. A through computational procedure by DFT/TD-DFT supports the experimental results of X-ray analyses and electronic spectra.

Supplementary materials

IR and EI-mass spectra for compounds **1**-**4** (Figs. S1 and S2). ^{1}H NMR spectra for 1 and 3 (Figs. S3). ^{1}H NMR spectra for **1** with NaCN (Fig. S4). UV-vis. spectra for **1, 3** and **2** (Fig. S5). Simulated UV-vis. spectra for **1** and **3** using different combinations of the functionals and the basis sets (Figs. S6). Optimized structures for **1, 3** and **4** (Fig. S7). Molecular structures for **1, 3** and **4** with full atom labeling (Fig. S8). Supramolecular Packing analysis for **1** (Tables S1 and S2). Excited states, excitation energy (eV), wavelength (nm) and oscillator strength (*f*) for **1** and **3** with PCM in chloroform (Tables S3 and S4).

CRediT authorship contribution statement

Mohammed Enamullah: Conceptualization, Methodology, Validation, Formal analysis, Investigation, Resources, Data curation, Writing – original draft, Writing – review & editing, Visualization, Supervision, Project administration, Funding acquisition. **Imdadul Haque:** Formal analysis, Investigation, Data curation, Writing – review & editing. **Afsana Mim:** Formal analysis, Investigation, Data curation. **Mohammad Khairul Islam:** Formal analysis, Data curation. **Baldeep K. Sidhu:** Formal analysis, Data curation. **David E. Herbert:** Resources, Writing – review & editing, Visualization. **Dennis Woschko:** Formal analysis, Investigation, Data curation. **Christoph Janiak:** Conceptualization, Validation, Resources, Writing – review & editing, Visualization, Project administration, Funding acquisition.

Declaration of Competing Interest

The authors declare that they have no known competing financial interests or personal relationships that could have appeared to influence the work reported in this paper.

Data availability

Data will be made available on request.

Acknowledgments

We acknowledge Wazed Miah Science Research center (WMSRC) at Jahangirnagar University, Bangladesh for obtaining CV data. The authors acknowledge the financial support from the Alexander von Humboldt Foundation (AvH), Bonn, Germany under the Research Group Linkage Program. For computational resource, we thank Professor ABP Lever, Department of Chemistry, York University, Toronto and the computecanada.ca (https://ccdb.computecanada.ca) Ontario, Canada. The Canada Foundation for Innovation and Research Manitoba (#32146) are thanked for support of purchase of an X-ray diffractometer (DH). The Rigaku X-ray diffractometer was funded by DFG through grant 440366605 (to CJ). The authors also thank the Center for Molecular and Structural Analytics at Heinrich Heine University (CeMSA@HHU) for recording the mass spectrometric data.

Supplementary materials

Supplementary material associated with this article can be found, in the online version, at doi:10.1016/j.molstruc.2023.136078.

References

[1] C. Evans, D. Luneau, New Schiff base zinc(II) complexes exhibiting second harmonic generation, J. Chem. Soc. Dalton Trans. (2002) 83–86.

[2] S.E. Howson, P. Scott, Comments on synthesis and characterization of enantiopure copper(II) complexes with chiral bidentate ligands, Dalton Trans. 40 (2011) 4332–4333.

[3] H. Sakiyama, H. Okawa, N. Matsumoto, S. Kida, Stereoselectivity in diastereomeric tetrahedral metal(II) complexes of chiral salicylideneamincs: crystal structure and molecular mechanics calculation of bis[N-(l-methyl)salicylideneaminato]cobalt (II), Bull. Chem. Soc. Jpn. 64 (1991) 2644–2667.

[4] H. Sakiyama, H. Okawa, N. Matsumoto, S. Kida, A tetrahedral zinc(II) complex of *N*-(*R*)-1-phenylethylsalicylideneimine. Structural and circular dichroism spectral investigations on stereoselectivity, J. Chem. Soc. Dalton Trans. (1990) 2935–2939.

[5] O. Mamula, A. von Zelewsky, T. Bark, H. Stoeckli-Evans, A. Neels, G. Bernardinelli, Predetermined chirality at metal centers of various coordination geometries: a chiral cleft ligand for tetrahedral (t-4), square-planar (sp-4), trigonal-bipyramidal (tb-5), square-pyramidal (spy-5), and octahedral (oc-6) complexes, Chem. Eur. J. 6 (2000) 3575–3585.

[6] T. Akitsu, Photofunctional supramolecular solution systems of chiral Schiff base nickel(II), copper(II) and zinc(II) complexes and photochromic azobenzenes, Polyhedron 26 (2007) 2527–2535.

[7] T. Akitsu, T. Itoh, Polarized spectroscopy of hybrid materials of chiral Schiff base cobalt(II), nickel(II), copper(II), and zinc(II) complexes and photochromic azobenzenes in PMMA films, Polyhedron 29 (2010) 477–487.

[8] C.E. Satheesh, P.R. Kumar, N. Shivakumar, K. Lingaraju, P.M. Krishna, H. Rajanaika, A. Hosamani, Synthesis, structural characterization, antimicrobial and DNA binding studies of homoleptic zinc and copper complexes of NO Schiff bases derived from homoveratrylamine, Inorg. Chim. Acta 495 (2019), 118929.

[9] J.M. Fernandez-G, O.L. Ruiz-Ramirez, R.A. Toscano, N. Macias-Ruvalcaba, M. Aguilar-Martinez, Crystal structures and voltammetric behavior of three copper (II) complexes derived from bulky Schiff bases, Transit. Met. Chem. 25 (2000) 511–517.

[10] Ş.P. Yalçın, Ü. Ceylan, M. Sönmez, M.E. Hacıyusufoğlu, H. Karavelioğlu, Synthesis, electron paramagnetic resonance studies and molecular calculations of N-aminopyrimidine salicylaldiminato copper(II) complex, J. Mol. Struct. 1147 (2017) 12–21.

[11] H. Brunner, R. Oeschey, B. Nuber, Synthesis, properties, stereochemistry and crystal structures of diastereomeric benzene–ruthenium(II) complexes with a chiral salicylideneaminato ligand, J. Chem. Soc. Dalton Trans. (1996) 1499–1508.

[12] I. Karamé, M. Jahjah, A. Messaoudi, M.L. Tommasino, M. Lemaire, New ruthenium catalysts containing chiral Schiff bases for the asymmetric hydrogenation of acetophenone, Tetrahedron: Asymmetry 15 (2004) 1569–1581.

[13] Z.H. Yang, L.X. Wang, Z.H. Zhou, Q.L. Zhou, C.C. Tang, Synthesis of new chiral Schiff bases and their application in the asymmetric trimethylsilylcyanation of aromatic aldehydes, Tetrahedron: Asymmetry 12 (2001) 1579–1582.

[14] C. Gan, G. Lai, Z. Zhang, Z. Wang, M.M. Zhou, Efficient and enantioselective nitroaldol reaction catalyzed by copper Schiff-base complexes, Tetrahedron: Asymmetry 17 (2006) 725–728.

[15] M. Itagaki, K. Hagiya, M. Kamitamari, K. Masumoto, K. Suenobu, Y. Yamamoto, Highly efficient chiral copper Schiff-base catalyst for asymmetric cyclopropanation of 2,5-dimethyl-2,4-hexadiene, Tetrahedron 60 (2004) 7835–7843.

[16] M. Enamullah, A.K.M. Royhan Uddin, G. Pescitelli, R. Berardozzi, G. Makhloufi, V. Vasylyeva, A.C. Chamayou, C. Janiak, Induced chirality-at-metal and diastereoselectivity at Δ/Λ-configured distorted square-planar copper complexes by enantiopure Schiff base ligands: combined circular dichroism, DFT and X-ray structural studies, Dalton Trans. 43 (2014) 3313–3329.

[17] M. Górecki, M. Enamullah, M.A. Islam, M.K. Islam, S.P. Höfert, D. Woschko, C. Janiak, G. Pescitelli, Synthesis and characterization of bis[(*R* or *S*)-N-1-(X-C_6H_4) ethyl-2-oxo-1-naphthaldiminato-κ^2N,O]-Λ/Δ-cobalt(II) (X = H, *p*-CH_3O, *p*-Br) with symmetry- and distance-dependent vibrational circular dichroism enhancement and sign inversion, Inorg. Chem. 60 (2021) 14116–14131.

[18] M. Enamullah, G. Makhloufi, R. Ahmed, B.A. Joy, M.A. Islam, D. Padula, H. Hunter, G. Pescitelli, C. Janiak, Synthesis, X-ray, and spectroscopic study of dissymmetric tetrahedral zinc(II) complexes from chiral Schiff base naphthaldiminate ligands with apparent exception to the ECD excitation chirality, Inorg. Chem. 55 (2016) 6449–6464.

[19] M. Enamullah, K.S. Banu, M.A. Hossain, Ü. Kökçam-Demir, High-spin bis[(*S* or *R*)-N-1-(Ar)ethyl-salicylaldiminato-κ^2N,O]-Λ/Δ-iron(II): combined studies of syntheses, spectroscopy, diastereoselection, electrochemistry, paramagnetic, thermal, PXRD and DFT/TDDFT, J. Mol. Struct. 1199 (2020), 126947.

[20] M. Enamullah, M.M. Rahman, M.K. Islam, D. Woschko, C. Janiak, G. Pescitelli, Characterization of diastereomeric equilibria of pseudotetrahedral bis[(*R* or *S*)-N-1-(Ar)ethylsalicylaldiminato-κ^2N,O]zinc(II) with Λ/Δ-chirality induction at-metal, ChemistryOpen 11 (2022), e202200116.

[21] G. Pescitelli, S. Lüdeke, A.C. Chamayou, M. Marolt, V. Justus, M. Górecki, L. Arrico, L. Di Bari, M.A. Islam, I. Gruber, M. Enamullah, C. Janiak, Broad-range spectral analysis for chiral metal coordination compounds: (chiro)optical superspectrum of cobalt(II) complexes, Inorg. Chem. 57 (2018) 13397–13408.

[22] N. Kordestani, H.A. Rudbaria, G. Bruno, S. Rosario, J.D. Braun, D.E. Herbert, O. Blacque, I. Correia, M. Al-M. Zaman, M.M. Bindu, C. Janiak, M. Enamullah, Solid-state to solution helicity inversion of pseudotetrahedral chiral copper(II) complexes with 2,4-dihalo-salicylaldiminate ligands, Dalton Trans. 49 (2020) 8247–8264.

[23] M. Enamullah, M.A. Hossain, M.K. Islam, D. Woschko, C. Janiak, Pseudotetrahedral copper(II)-complexes with enantiopure (*R* or *S*)-2-(((aryl) ethylimino)ethyl)phenolate Schiff base ligands, Dalton Trans. 50 (2021) 9236–9249.

[24] M. Enamullah, M. Al-M. Zaman, M.M. Bindu, D. Woschko, M.K. Islam, C. Janiak, Pseudotetrahedral high-spin manganese(II)-complexes with (*S* or *R*)-N-1-(Ar)ethyl-salicylaldimine: chiroptical property, chirality induction at-metal, paramagnetism, redox-potential, PXRD structures and DFT/TDDFT, J. Mol. Struct. 1239 (2021), 130455.

[25] H.A. Rudbari, A. Saadati, M. Aryaeifar, O. Blacque, I. Correia, M.K. Islam, C. Janiak, M. Enamullah, Pseudotetrahedral Zn(II)-(*R* or *S*)-dihalogen-salicylaldiminato complexes with Λ- or Δ-chirality induction at-metal, Dalton Trans. 51 (2022) 2385–2399.

[26] M. Enamullah, M. Al-M. Zaman, M.M. Bindu, M.K. Islam, M.A. Islam, Experimental and theoretical studies on isatin-Schiff bases and their copper(II)-complexes: syntheses, spectroscopy, tautomerism, redox potentials, EPR, PXRD and DFT/TDDFT, J. Mol. Struct. 1201 (2020), 127207.

[27] A. von Zelewsky, Stereochemistry of Coordination Compounds, John Wiley & Sons, Chichester, 1996, p. 69.

[28] E.C. Constable, G. Zhang, C.E. Housecroft, M. Neuburger, J.A. Zampese, π-Stacking and hydrogen bonding direct diastereoselectivity in one-pot syntheses of octahedral iron (II) complexes, Chem. Commun. 46 (2010) 3077–3079.

[29] R.E. Ernst, M.J. O'Connor, R.H. Holm, Diastereoisomeric four-coordinate complexes. III. Paramagnetic nickel(II) complexes with three asymmetric centers, J. Am. Chem. Soc. J 89 (24) (1967) 6104–6113.

[30] T. Akitsu, Y. Einaga, Synthesis and crystal structures of the flexible Schiff base complex bis(N-1,2-diphenylethyl-salicydenaminato-κ^2N,O)copper(II) (methanol): a rare case of solvent-induced distortion, Polyhedron 25 (2006) 1089–1095.

[31] T. Akitsu, Y. Einaga, Syntheses, crystal structures and electronic properties of a series of copper(II) complexes with 3,5-halogen-substituted Schiff base ligands and their solutions, Polyhedron 24 (2005) 2933–2943.

[32] Z. Dezhahang, M.R. Poopari, J. Cheramy, Y.J. Xu, Conservation of helicity in a chiral pyrrol-2-yl Schiff-base ligand and its transition metal complexes, Inorg. Chem. 54 (2015) 4539–4549.

[33] H. Gkawa, M. Nakamura, S. Kida, Noncovalent interactions in metal complexes. Stereoselectivity of tetrahedral or pseudotetrahedral bis(N-l-menthylsalicylaldiminato)M(II) and bis(N-l-menthyl-3-methylsalicylaldiminato)M (II) (M = Co, Cu, Ni, Zn), Inorg. Chim. Acta 120 (1986) 185–189.

[34] M. Enamullah, V. Vasylyeva, M.A. Quddus, M.K. Islam, S.P. Höfert, C. Janiak, Spontaneous resolution of a Δ/Λ-chiral-at-metal pseudo-tetrahedral Schiff-base zinc complex to a racemic conglomerate with C–H···O organized 41- and 43-helices, CrystEngComm 20 (2018) 4724–4734.

[35] M. Enamullah, M.A. Islam, B.A. Joy, B. Dittrich, G.J. Reiss, C. Janiak, π–π interaction leading to an inversion-symmetric complex pair of Λ- and Δ-*bis*[N-2-(R-pyridyl)-2-oxo-1-naphthaldiminato-κ^2*N,O*]zinc(II), Inorg. Chim. Acta 482 (2018) 935–942.

[36] M. Enamullah, I. Haque, A.K. Resma, D. Woschko, C. Janiak, Schiff-base in ketoamine form and Rh(η4-cod)-Schiff base complex with Z' = 2 structure from pairwise C-H···metallochelate-π contacts, Molecules 28 (2023) 172–192.

[37] A. Mim, M. Enamullah, I. Haque, A. Mohabbat, C. Janiak, Synthesis, molecular structure, mesomorphism and DFT/TDDFT calculations of square-planar bis[1-((*p*-tolylimino)methyl)naphthalen-2-olato-κ^2N,O]nickel or copper(II) complexes, J. Mol. Struct. 1291 (2023), 135669.

[38] K. Iwase, Y. Toyama, I. Yoshikawa, Y. Yamamura, K. Saito, H. Houjou, Insight into structural demand for cold crystallization of a small molecule. A case study for Schiff base compounds that exhibit prototropic tautomerization, Bull. Chem. Soc. Jpn. 91 (4) (2018) 669–677.

[39] W.G. Jia, Z.B. Wang, X.T. Zhi, J.Q. Han, Y. Sun, Syntheses, characterization and catalytic activities of half-sandwich ruthenium complexes with naphthalene-based Schiff base ligands, J. Coord. Chem. 70 (5) (2017) 848–858.

[40] A.F. Shoair, A.R. El-Shobaky, H.R. Abo-Yassin, Synthesis, spectroscopic characterization, catalytic and antibacterial studies of ruthenium(III) Schiff base complexes, J. Mol. Liq. 211 (2015) 217–227.

[41] CrysAlisPro, Rigaku Oxford Diffraction, Release 1.171.40.103a, 2021.

[42] G.M. Sheldrick, Crystal structure refinement with SHELXL, Acta Crystallogr. Sect. C C71 (2015) 3–8. Cryst. Struct. Commun.

[43] G.M. Sheldrick, A short history of SHELX, Acta Crystallogr. A Found. Crystallogr. A64 (2008) 112–122.

[44] O.V. Dolomanov, L.J. Bourhis, R.J. Gildea, J.A.K. Howard, H. Puschmann, OLEX2: a complete structure solution, refinement and analysis program, J. Appl. Crystallogr. 42 (2009) 339–341.

[45] K. Brandenburg, Diamond (Version 4.6), crystal and molecular structure visualization, crystal impact - K. Brandenburg & H. Putz Gbr, Bonn, Germany, (2009-2022).

[46] A.L. Spek, PLATON, An integrated tool for the analysis of the results of a single crystal structure determination, Acta Crystallogr. A46 (1990) C34.

[47] A.L. Spek, PLATON - a multipurpose crystallographic tool, Utrecht University, Utrecht, The Netherlands, 2005.

[48] A.L. Spek, Structure validation in chemical crystallography, Acta Crystallogr. D65 (2009) 148–155.

[49] L.J. Farrugia, Windows implementation, Version 270519 (University of Glasgow, Scotland) 2019.

[50] Bruker-AXS. APEX4 V2021.10-0. 2021.

[51] A. Altomare, C. Giacovazzo, A. Guagliardi, A.G.G. Moliterni, R. Rizzi, P.E. Werner, New techniques for indexing: N-TREOR in EXPO, J. Appl. Crystallogr. 33 (2000) 1180–1186.

[52] D. Louër et R. Vargas, Indexation automatique des diagrammes de poudre par dichotomies successives, J. Appl. Crystallogr. 15 (1982) 542–545.

[53] A. Altomare, C. Cuocci, C. Giacovazzo, A. Moliterni, R. Rizzi, N. Corriero, A. Falcicchio, EXPO2013: A kit of tools for phasing crystal structures from powder data, J. Appl. Crystallogr. 46 (2013) 1231.
[54] M.J. Frisch, G.W. Trucks, H.B. Schlegel, G.E. Scuseria, M.A. Robb, J.R. Cheeseman, G. Scalmani, V. Barone, G.A. Petersson, H. Nakatsuji, X. Li, M. Caricato, A.V. Marenich, J. Bloino, B.G. Janesko, R. Gomperts, B. Mennucci, H.P. Hratchian, J.V. Ortiz, A.F. Izmaylov, J.L. Sonnemberg, D. Williams-Young, F. Ding, F. LIpparini, F. Egidi, J. Goings, B.Peng, A.Petrone, T.Henderson, D.Ranasinghe, V.G. Zakrzewski, J. Gao, N. Rega, G. Zheng, W. Liang, M. Hada, M. Ehara, K. Toyota, R. Fukuda, J. Hasegawa, M. Ishida, T. Nakajima, Y. Honda, O. Kitao, H. Nakai, T. Vreven, K. Throssell, J.J.A. Montgomery, J.E. Peralta, F. Ogliaro, M. Bearpark, J.J. Heyd, E. Brothers, K.N. Kudin, V.N. Staroverov, T.A. Keith, R. Kobayashi, J. Normand, K. Raghavachari, A. Rendell, J.C. Burant, S.S. Iyengar, J. Tomasi, M. Cossi, J.M. llam, M. Klene, C. Adamo, R. Cammi, J.W. Ochterski, R.L. Martin, K. Morokuma, O. Farkas, J.B. Foresman, D.J. Fox, Gaussian 16, Revision A.03, Gaussian, Inc.: Wallingford CT, 2016, GaussView 5.0. Wallingford, E.U.A.
[55] T. Bruhn, A. Schaumlöffel, Y. Hemberger, G. Pescitelli, SpecDis Version 1.71, Berlin, Germany, 2017.
[56] A.F. Orchard, Magnetochemistry, Oxford University Press, Oxford, 2003.
[57] Y. Shibuya, K. Nabari, M. Kondo, S. Yasue, K. Maeda, F. Uchida, H. Kawaguchi, The copper (II) complex with two didentate Schiff base ligands. The unique rearrangement that proceeds under alcohol vapor in the solid state to construct noninclusion structure, Chem. Lett. 37 (2008) 78–79.
[58] L. Yang, D.R. Powell, R.P. Houser, Structural variation in copper(I) complexes with pyridylmethylamide ligands: structural analysis with a new four-coordinate geometry index, τ4, Dalton Trans. (2007) 955. -364.
[59] C. Janiak, A critical account on π–π stacking in metal complexes with aromatic nitrogen-containing ligands, J. Chem. Soc. Dalton Trans. (2000) 3885–3896.
[60] M. Nishio, CH/π hydrogen bonds in crystals, CrystEngComm 6 (2004) 130–158.
[61] M. Nishio, M. Hirota, Y. Umezawa, The CH/π Interaction (Evidence, Nature and Consequences), Wiley-VCH, 1998.
[62] Y. Umezawa, S. Tsuboyama, K. Honda, J. Uzawa, M. Nishio, CH/π Interaction in the crystal structure of organic compounds. A database Study, Bull. Chem. Soc. Jpn. 71 (1998) 1207–1213.
[63] N.N.L. Madhavi, A.K. Katz, H.L. Carrell, A. Nangia, G.R. Desiraju, Evidence for the characterisation of the C–H···π interaction as a weak hydrogen bond: toluene and chlorobenzene solvates of 2,3,7,8-tetraphenyl-1,9,10-anthyridine, Chem. Commun. (1997) 1953–1954.
[64] T. Steiner, M. Tamm, B. Lutz, J. van der Maas, First example of cooperative O–H···CC–H···Ph hydrogen bonding: crystalline 7-ethynyl-6,8-diphenyl-7*H*-benzocyclohepten-7-ol, Chem. Commun. (1996) 1127–1128.